Acta Crystallographica Section D
Biological Crystallography
ISSN 0907-4449

Structure of the C-terminal sterile α-motif (SAM) domain of human p73α

Wooi Koon Wang, Mark Bycroft, Nicholas W. Foster, Ashley M. Buckle, Alan R. Fersht and Yu Wai Chen*

Centre for Protein Engineering and Cambridge University Chemical Laboratory, MRC Centre, Hills Road, Cambridge CB2 2QH, England

Correspondence e-mail: ywc@mrc-lmb.cam.ac.uk

Received 16 November 2000
Accepted 5 February 2001

PDB Reference: p73α SAM domain, 1dxs.

p73 is a homologue of the tumour suppressor p53 and contains all three functional domains of p53. The α-splice variant of p73 (p73α) contains near its C-terminus an additional structural domain known as the sterile α-motif (SAM) that is probably responsible for regulating p53-like functions of p73. Here, the 2.54 Å resolution crystal structure of this protein domain is reported. The crystal structure and the published solution structure have the same five-helix bundle fold that is characteristic of all SAM-domain structures, with an overall r.m.s.d. of 1.5 Å for main-chain atoms. The hydrophobic core residues are well conserved, yet some large local differences are observed. The crystal structure reveals a dimeric organization, with the interface residues forming a mini four-helix bundle. However, analysis of solvation free energies and the surface area buried upon dimer formation indicated that this arrangement is more likely to be an effect of crystal packing rather than reflecting a physiological state. This is consistent with the solution structure being a monomer. The p73α SAM domain also contains several interesting structural features: a Cys-*X*-*X*-Cys motif, a 3_{10}-helix and a loop that have elevated *B* factors, and short tight inter-helical loops including two β-turns; these elements are probably important in the normal function of this domain.

1. Introduction

It once seemed that *p53* was a lone gene without a family, in contrast to other tumour-suppressor genes and oncogenes. However, in 1997 Kaghad and coworkers reported their accidental discovery of *p73*, a close relative of *p53* (Kaghad *et al.*, 1997). This was followed immediately by the cloning of *p63* (Yang *et al.*, 1998). *p63* and *p73* both share high sequence homology with *p53* and the translated amino-acid sequences have domain structures closely resembling that of p53 and contain the transcription-activation, DNA-binding and tetramerization domains. As expected, the two proteins p63 and p73 can activate p53-transcription target sequences (Jost *et al.*, 1997; Kaghad *et al.*, 1997; Yang *et al.*, 1998). However, p63 and p73 are probably not tumour suppressors. While they do share some overlapping functions with p53, their normal roles seem to be more involved with regulation of development processes (for recent reviews, see Kaelin, 1999; Levrero *et al.*, 2000; Lohrum & Vousden, 2000; Marin & Kaelin, 2000).

Whereas *p53* encodes a unique gene product, the *p73* gene produces at least six isoforms, α, β, γ, δ, ε and ζ (Kaghad *et al.*, 1997; De Laurenzi *et al.*, 1998; Ueda *et al.*, 1999; Zaika *et al.*, 1999). All variants contain the three common p53-like domains encoded by exons 2–10. Various alternative splicing schemes in sequences beyond exon 10 produce p73 proteins with different C-termini. *p63* also encodes at least three

Table 1
Crystallographic data and refinement statistics for p73α SAM domain.

Crystal information	
Space group	$P4_12_12$
Unit-cell parameters (Å)	
$a = b$	32.02
c	133.84
Refinement statistics	
Resolution range (Å)	26–2.54
R_{cryst}† (%)	27.5
R_{free}‡ (%)	34.6
No. of protein atoms	441
No. of water atoms	26
Average B factor (Å^2)	
Predicted from Wilson plot	59.4
All atoms	58.6
Overall (protein)	57.1
Main chain	53.4
Side chain	55.2
Water molecules	64.0
R.m.s. deviation from ideality	
Bonds (Å)	0.007
Bond angles (°)	1.2
Dihedrals (°)	20.4
Improper angles (°)	0.71
Estimated coordinate error (Å)	
Luzzati plot	0.42
From σ_A	0.42
Ramachandran plot§	
In most favoured region (%)	87.5
In additional allowed region (%)	12.5
In generously allowed/disallowed regions (%)	0.0
Overall G factor§	0.35

† $R_{cryst} = \sum ||F_o| - |F_c|| / \sum |F_o|$, where F_o and F_c are the observed and calculated amplitudes, respectively. ‡ The R_{free} set contains 10.2% of total reflections. § Results from *PROCHECK*.

proteins that show similar splicing variations at the C-terminus (Yang *et al.*, 1998).

The α-splice variant of p73 (p73α) is the full-length gene product and is the most abundantly expressed isoform. It is unique in not exhibiting efficient homotypic interactions (Kaghad *et al.*, 1997; De Laurenzi *et al.*, 1998), despite containing a functional tetramerization domain (Davison *et al.*, 1999). p73α has reduced activities in transactivation of p53-responsive targets compared with p73β (exon 13 spliced out) and p53 (Jost *et al.*, 1997; Kaghad *et al.*, 1997; De Laurenzi *et al.*, 1998).

p73α harbours 216 C-terminal residues that do not have homologous partners in p53. Interestingly, a structural module of around 70 residues known as the sterile α-motif (SAM) has been identified within this region (Ponting, 1995; Thanos & Bowie, 1999). SAM domains are present predominantly in either termini of a diverse range of proteins that are involved in developmental regulation and signal transduction. This module is considered to be responsible for expanding or regulating protein functions *via* self-association, by association with other SAM domains or with other protein modules (for a review, see Schultz *et al.*, 1997). The SAM domain of p73α is probably a similar regulatory element and accounts for the functional differences between p73α and p73β (Ozaki *et al.*, 1999). The α-splice variant of p63 (p63α) is highly homologous with p73α and also contains a SAM domain.

Because of its biological interest, we set out to determine the crystal structure of the SAM domain of p73α, containing residues 487–564 and hereafter referred to as p73α-SAM. The structure of a monomeric ten-residue shorter construct, p73α residues 487–554, has been determined by nuclear magnetic resonance (NMR) spectroscopy (Arrowsmith, 1999; Chi *et al.*, 1999).

2. Experimental procedures

2.1. Crystallization and structure solution

The overproduction, purification and crystallization of recombinant p73α-SAM are described elsewhere (Wang *et al.*, 2000). The structure determination by molecular replacement using the NMR structure of p73α-SAM residues 487–554 (PDB entry 1cok; Chi *et al.*, 1999) as a search model has also been reported (Wang *et al.*, 2000).

2.2. Structure refinement

The molecular-replacement solution was subjected to alternating cycles of computational refinement and manual rebuilding. We employed torsional molecular dynamics (Rice & Brünger, 1994) implemented in the program *CNS* (Brunger *et al.*, 1998) using the maximum-likelihood target function. Throughout the course of refinement, 10% of the data was left out for cross validation and a bulk-solvent model was used. Only overall and grouped B factors (one for main-chain and one for side-chain atoms in each residue) were refined. Manual rebuilding was performed with the program *O* (Jones *et al.*, 1991) guided by σ_A-weighted maps with $2mF_o - DF_c$ and $mF_o - DF_c$ coefficients (Read, 1986), as well as maps generated by a density-modification protocol (Abrahams & Leslie, 1996). All maps were calculated with *CNS*. After seven rounds, the refinement essentially converged and the resulting model had an R factor of 0.27 and an R_{free} of 0.34 for all data to 2.54 Å. Further rebuilding and refinement resulting in a lower R factor but not accompanied by a lower R_{free} was regarded as overfitting. The quality of the final model was assessed with *PROCHECK* (Laskowski *et al.*, 1993) and found to be excellent (Table 1).

The high R factor and R_{free} are consistent with a large extent of disorder (23 residues of 80). There is sufficient volume to accommodate these missing residues (seven at the N-terminus and 16 at the C-terminus) in the crystal lattice. We modelled dummy residues into the empty volumes at both termini and generated a solvent mask excluding these volumes. With this solvent mask, we performed density modification with the program *DM* (Collaborative Computational Project, Number 4, 1994; Cowtan, 1994). We also computed a maximum-entropy map with the program *BUSTER* (Buster Development Group, 2001). Neither of these methods revealed interpretable electron density for rebuilding the missing terminal atoms. These results are consistent with the unstructured ends observed in the NMR structure. We therefore concluded that

these residues are truly disordered and that refinement was complete despite the R factor and R_{free} remaining high.

2.3. Analytical ultracentrifugation

Sedimentation equilibrium experiments were carried out with a Beckman Optima XL-I analytical ultracentrifuge equipped with an An-50 Ti rotor. Protein samples were prepared in 20 mM Tris–HCl pH 7.5, 150 mM NaCl at three initial concentrations: 38, 52 and 70 μM. Experiments were run at 12 500 rev min^{-1} at 293 K, scanning at 276 nm. Data sets were collected at 24 h intervals until equilibrium was reached. The program *SEDNTERP* (Laue *et al.*, 1992) was used to calculate the partial specific volume and solvent density from the amino-acid and buffer compositions to be 0.732 ml g^{-1} and 1.005 g ml^{-1}, respectively. Mass average apparent molecular weights were calculated as previously described by Poget *et al.* (1999). Data was also analysed using the program *ULTRASPIN* (Veprinstev, Foster & Fersht, manuscript in preparation).

3. Results

3.1. Quality of structure model

The final model of p73α-SAM consists of residues 492–548. The $2mF_o - DF_c$ map shows well defined electron density without any break in the backbone. The real-space correlation coefficient (Jones *et al.*, 1991) of each residue was calculated with *O* to assess the quality of the structure model and these are shown in Fig. 1. A high overall value of 0.85 indicated that the model is a good interpretation of the diffraction data. The mean B factor for the protein atoms is 57.1 Å^2 and agrees well with the B factor of 59.4 Å^2 derived from the Wilson plot. The first seven N-terminal residues, including two plasmid-encoded residues and residues 487–491, and the C-terminal residues 549–564 are disordered. Some side-chain atoms of residues Ser492, His519, Gln521, Gln536 and Leu548 could also not be modelled into the electron-density map and are therefore omitted from the model.

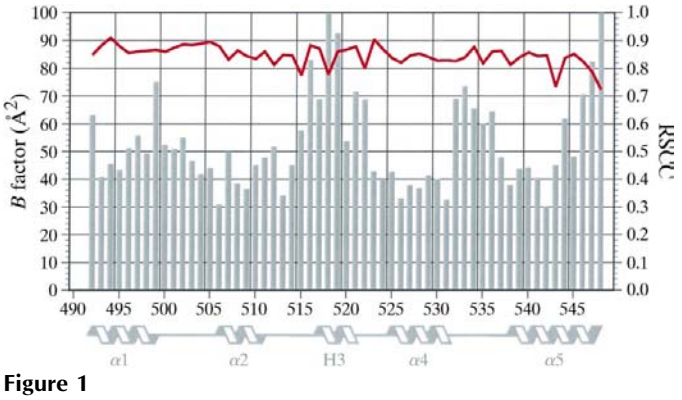

Figure 1
Real-space correlation coefficient (RSCC, red line) calculated using the $2mF_o - DF_c$ map and main-chain B factors (grey bars) of the p73α-SAM crystal structure. The secondary structure is illustrated at the bottom for reference.

3.2. Overall structure

The crystal structure of p73α-SAM has the same topology as the previously reported NMR structure (Chi *et al.*, 1999) and other SAM-domain structures (Slupsky *et al.*, 1998; Smalla *et al.*, 1999; Stapleton *et al.*, 1999; Thanos, Faham *et al.*, 1999; Thanos, Goodwill *et al.*, 1999) and consists of helix 1 (α1, residues 492–499), loop 1 with a type I β-turn (residues 502–505), helix 2 (α2, residues 506–511), loop 2, 3_{10}-helix 3 (H3, residues 517–521), loop 3, helix 4 (α4, residues 525–531), loop 4 with another type I β-turn (residues 534–537) and finally helix 5 (α5, residues 538–548). The helices pack tightly to form a compact globular unit. According to the Dali/FSSP server (Holm & Sander, 1996; http://www.ebi.ac.uk/dali), this structure belongs to the five-helix bundle family. The closest relatives are SAM domains of the Ephrin (Eph) receptor tyrosine kinases and the Ets-1 pointed domain (Slupsky *et al.*, 1998). Other close structural neighbours include the barrier-to-autointegration factor, endonuclease III and Holliday junction binding protein RuvA.

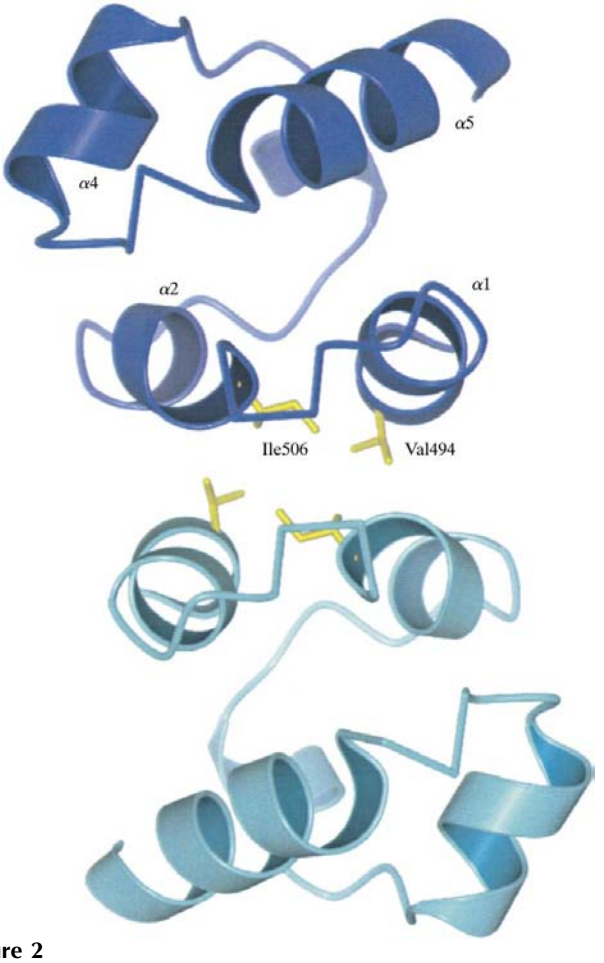

Figure 2
The crystallographic dimer of p73α-SAM. This view is down the twofold axis with which the dimer is generated. Each monomer is coloured individually. Residues Val494 and Ile506 are involved in the dimeric interface and are shown in yellow. This figure and Figs. 4, 5 and 6 were created with *BOBSCRIPT* (Esnouf, 1997) and rendered with *Raster3D* (Merritt & Bacon, 1997) or with *GL_RENDER* (Esser & Deisenhofer, unpublished program).

3.3. Oligomeric state

In the crystal lattice, each p73α-SAM molecule forms a dimer with a symmetry-equivalent neighbour related by a twofold rotation (Fig. 2). The dimeric interface is formed by two helices (α1 and α2) contributed by each monomer, resulting in a four-helix mini core containing four hydrophobic residues, Val494 and Ile506 from each monomer. The side chain of other residues on the surface of helices α1 and α2 (Thr498, Pro503, Glu507 and Thr510) also contribute to van der Waals packing between the two monomers. It is interesting to determine if this dimer reflects a physiological SAM–SAM association or if this is a result of crystal packing. The structure was analysed with the Protein Quaternary Structure server (PQS; http://pqs.ebi.ac.uk; Henrick & Thornton, 1998). The solvent-accessible surface area that is buried upon dimer formation is 327 Å^2 per monomer molecule. This is below the threshold value of 400 Å^2 used by PQS to classify a true dimer. A more recent study using a non-redundant structure database indicated that no known physiological dimer has a contact surface area of less than 500 Å^2, whereas the optimum cutoff for discriminating monomers and dimers is 856 Å^2 (Ponstingl *et al.*, 2000). The gain in solvation free energy upon dimer formation is only -26.4 kJ mol^{-1} for the 114 residues in the dimer. These results suggest that the dimeric arrangement is more likely to be a crystal packing artefact.

We employed analytical ultracentrifugation to confirm our results. The results of sedimentation equilibrium experiments indicated that p73α-SAM is essentially a monomer, shown in Fig. 3(*a*), with no evidence of dimerization even at the highest protein concentration (70 μM). A monomer model was employed and shows good fits to the sedimentation absorbance data at various radii of each cell, shown in Fig. 3(*b*); the apparent molecular weight obtained, 9197 Da, is in excellent agreement with the calculated molecular weight of 9018 Da.

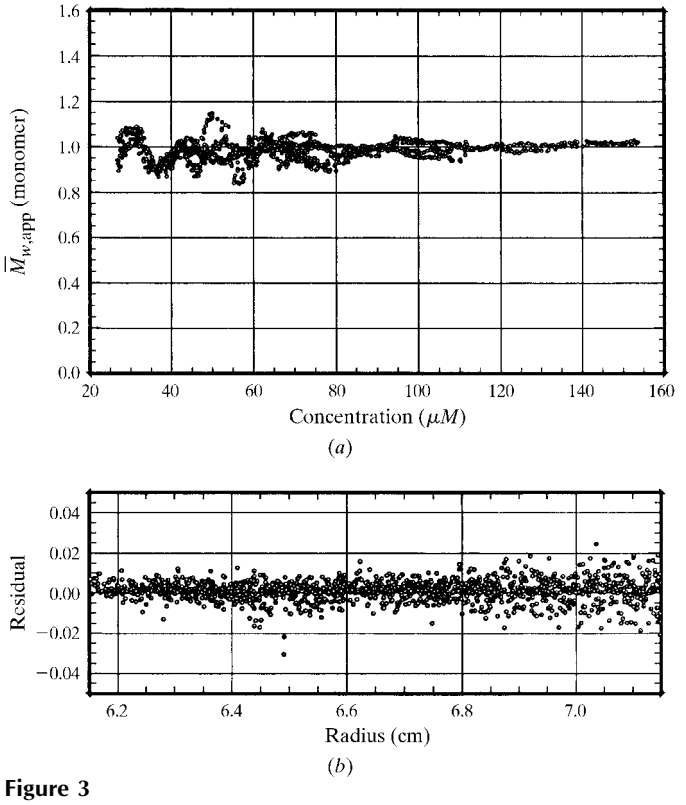

Figure 3
Sedimentation equilibrium analysis of p73α-SAM. (*a*) Plot of the mass apparent average molecular weight $\overline{M}_{w,\mathrm{app}}$ (as monomers of the sequence-derived molecular mass) against concentration for samples of p73α-SAM analysed at 293 K. Data from the samples at initial concentrations of 38, 52 and 70 μM are plotted together to show the extent of overlap. (*b*) Residual errors between the measured optical density and that calculated from direct fitting to a model for the formation of monomers, optimizing the baseline error and monomer molecular mass for each sample. The model fits well to the data over the radii used, showing a relatively even distribution of residual errors around zero lines.

3.4. Comparison with NMR structure

The crystal structure of p73α-SAM can be aligned with the solution structure (best representative model 7) with an overall root-mean-square deviation (r.m.s.d.) of 1.47 Å for the main-chain atoms of residues 492–548 (Fig. 6). This is similar to the difference between the crystal and NMR structures of EphB2-SAM of 1.4 Å and falls within the range commonly observed when a crystal structure and an NMR structure of the same protein are compared (Chen *et al.*, 2000). We compared the crystal and NMR structures by calculating an error-scaled difference distance matrix (DDM) with the program *ESCET* (Schneider, 2000) between all C$^\alpha$ atoms. The DDM revealed in detail local differences and similarities of the two structures (results not shown). The best conserved region is defined by the C-terminal residues 535–548 (second β-turn plus helix α5). The second largest conserved region is defined by the N-terminal residues 492–502 (helix α1 plus three loop residues). These structural differences are the results of subtle changes in the relative positions of the secondary-structure elements. Noticeably, two regions, residues 496–502 (last turn of α1 plus 2–3 loop residues) and residues 509–514 (last turn of α2 plus three loop residues), are each more distant from the rest of the structure in the NMR structure. H3, the helix with higher *B* factors (see later), is displaced relative to the N-terminal residues (α1, α2) but not to the C-terminal residues (α4, α5) in the two structures.

All residues in the crystal and NMR structures of p73α-SAM have similar solvent accessibility, except for two residues (see later). The residues that constitute the hydrophobic core are generally conserved in the crystal and NMR structures. In addition to those reported in the NMR study, namely Leu497, Leu500, Ile506, Phe509, Leu520, Leu528, Ile541, Trp542 and Leu545, we also found Leu493 and Ile533 contributing to the core. On the other hand, Leu514, a buried residue in the NMR structure, becomes partially exposed in the crystal structure (solvent accessibility increased from 3 to 25%). Another residue with a large increase in solvent accessibility is Gly513 (crystal, 77%; NMR, 18%). These two residues reside in loop 2, where the largest local atomic r.m.s.d. (approaching 3 Å) occurs.

3.5. Comparison with other SAM-domain structures

The overall alignments of the crystal structures of p73α-SAM and the SAM domains of the Eph receptor family are very good, with r.m.s.d. in C^{α} positions ranging from 1.6 to 1.9 Å. Although the amino-acid sequence identity is only 14–17% (Chi *et al.*, 1999), the SAM domains of the Eph receptors and that of p73 are close structural relatives.

3.6. Helix 3 and loop 4 have high *B* factors

The variation of backbone *B* factors in the p73α-SAM structure is illustrated in Figs. 1 and 4. Noticeably, residues in the small 3_{10}-helix (H3) and loop 4 (with the second β-turn) have higher *B* factors compared with the overall main-chain *B* factor of 53.4 Å^2. The average main-chain atomic *B* factor for H3 and two trailing loop residues (residues 516–522) is 76.8 Å^2 and that for loop 4 residues (residues 532–536, including the second β-turn) is 66.4 Å^2. Despite the high *B* factors, the $2mF_o - DF_c$ electron-density maps for these regions are well defined and continuous and agree well with the structure model, at least for the protein backbone.

3.7. A potential disulfide bridge

The two cysteine residues in the first β-turn, Cys502 and Cys505, are in good positions to from a disulfide bridge. A disulfide bond was modelled in the early rebuilding rounds. However, the resulting electron-density maps and subsequent refinement did not support the presence of this disulfide bond, as shown in Fig. 5. Presumably, this is because our protein samples were prepared in reducing conditions (with 5 m*M* β-mercaptoethanol). We tried growing crystals in conditions free of the reducing agent, but without success (Wang & Chen, unpublished results).

4. Discussion

4.1. SAM domain as a protein–protein interaction module

The self-association of SAM domains has been known for some time to play a regulatory role in proteins involved in the regulation of developmental processes (Schultz *et al.*, 1997). The structural evidence of this homotypic oligomerization has been provided by two crystal structures of the SAM domains derived from the Eph receptor tyrosine kinases (Stapleton *et al.*, 1999; Thanos, Goodwill *et al.*, 1999). In these two cases, large amounts of surface area are buried: 950 and 625 Å^2 per monomer for the two interaction sites involved in oligomer formation of EphB2-SAM and 962 Å^2 per monomer for dimerization of EphA4-SAM. However, homo-oligomerization is not observed in the two SAM-domain solution structures (Chi *et al.*, 1999; Smalla *et al.*, 1999). Recently, EphB2-SAM was shown to crystallize in an alternative crystal form as a monomer (Thanos, Faham *et al.*, 1999). Other non-structural methods such as analytical ultracentrifugation also indicated that the Eph receptor SAM domains are monomeric in solution even at high concentrations (Thanos, Faham *et al.*, 1999). These recent results cast doubts on the proposed modes of oligomerization based on the two Eph receptor SAM domain crystal structures.

We also found that p73α-SAM does not homo-oligomerize. This is supported by dynamic light-scattering experiments (Wang *et al.*, 2000) and equilibrium sedimentation experiments and is in total agreement with the results of Chi *et al.* (1999) on p73α-SAM residues 487–554. Homotypic association of the p73α-SAM domain, if there is any, must be very weak and is unlikely to play any regulatory role. However, it should be noted that heterotypic SAM–SAM interactions are known for some other proteins (Schultz *et al.*, 1997) and it is possible that other SAM-containing proteins can be recruited to perform regulatory functions on p73.

It is equally possible that p73α-SAM may interact with other protein modules. EphB1-SAM has been shown to bind to the Src homology 2 (SH2) domain upon phosphorylation (Stein *et al.*, 1996). Residue Tyr929 of EphB1-SAM, the phosphorylation site that is conserved among the Eph SAM domains, is not conserved in p73α-SAM. If there is any interaction with the SH2 domain, the phosphorylation site must be located elsewhere. Another possibility is that p73α-SAM binds to another region of p73, *e.g.* the tetramerization domain, and mediates negative regulation (Thanos & Bowie, 1999).

4.2. Unusual structural features

The p73α-SAM crystal structure has several interesting structural features that may be related to its cellular function.

All SAM domain structures are compact and contain loops of minimal length, just sufficient to make tight turns connecting the helices. These well defined loops seem to confer a very rigid skeleton upon the Eph SAM domains. p73α-SAM domain also has well defined residues in loop 1, loop 2 (except for a few residues connecting with H3) and loop 3. In the crystal structure, the *B* factors in these loop residues are similar to the overall average value (Figs. 1 and 4); in the NMR structure, the atomic r.m.s.d.s of these loop residues are similar to those of the flanking helices (not shown). Compared with the Eph SAM domains, p73α-SAM domain stands out as having some large variations in atomic *B* factors. The 3_{10}-helix H3 and loop 4 (between α4 and α5) have considerably higher *B* factors than the rest of the structure. In some cases, locally disordered regions observed in protein structures can be linked to biological functions (reviewed by Wright & Dyson, 1999). It is possible that the intrinsic flexibility of these regions have important functional implications, *e.g.* in adapting to an induced-fit docking conformation with other protein domains. This is consistent with the results of a parallel study of the backbone dynamics of this protein (Wang, Wong, Proctor, Bycroft, Nikolova, Freund and Fersht, manuscript in preparation).

The main-chain conformation of residues 502–505 (Cys-Pro-Asn-Cys) resembles that of an active-site Cys-*X*-*X*-Cys (C*XX*C) motif commonly found in the thioredoxin family (Martin, 1995; Guddat *et al.*, 1998), with the two cysteines within disulfide-bridge-forming distance, as shown in Fig. 5.

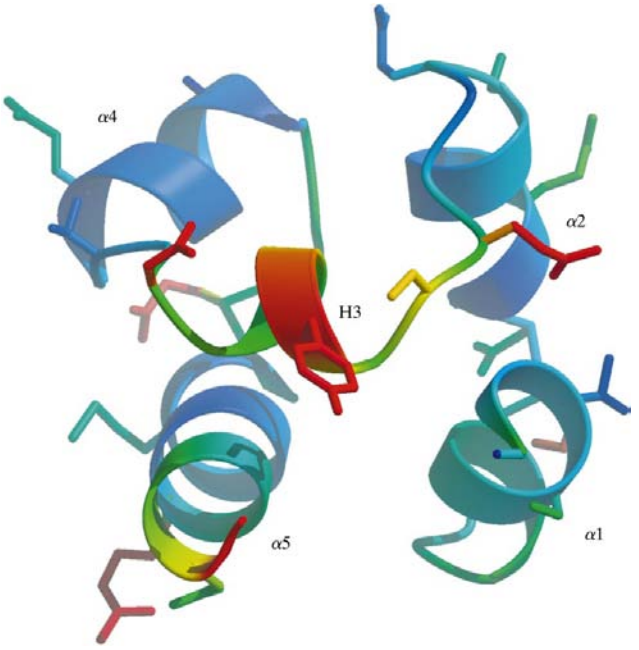

Figure 4
The overall structure of p73α-SAM, coloured according to the fluctuations in crystallographic *B* factors. Colour code: spectrally from red, the highest *B* factors, to green, intermediate and blue, the lowest.

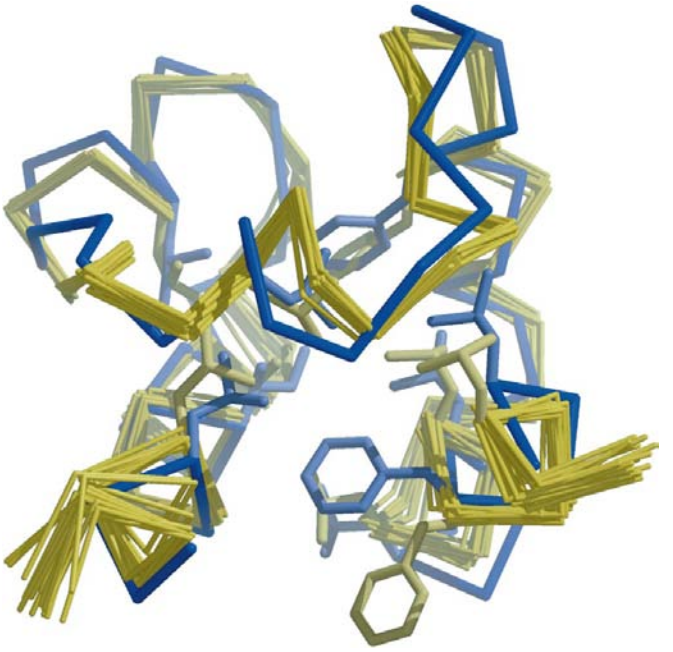

Figure 6
Comparison of crystal and NMR structures of p73α-SAM. The crystal structure is shown in blue and the NMR ensemble structure (models 1–15) is in yellow. The side chains of residues contributing to the hydrophobic core are shown.

Although the short sequence C*XX*C can be found in a variety of proteins of different functions, it is the catalytic C*XX*C motif in the thioredoxin family that has the closest match in conformation to that in p73α-SAM, having an r.m.s.d. in main-chain atomic positions of only 0.5 Å. Strikingly, this C*XX*C motif is also conserved in the p63α SAM-domain sequence (Cys523-Ser524-Ser525-Cys526) as well as in the SAM domains of some other relatives of the p53 family. By analogy with the functional significance of the C*XX*C motif in the thioredoxins, the SAM-domain C*XX*C motif of p73 may confer a similar oxidation–reduction catalytic role to this protein. Whether this is true or not has to be verified by further biochemical studies.

WKW is supported by a studentship from the Universiti Putra Malaysia and the Ministry of Science and Technology (Malaysia). YWC is supported by a Wellcome Trust Grant (061836). We would like to thank Kim Henrick for analyses using the PQS server. The Gérard Bricogne and Buster Development Group at the MRC LMB and GlobalPhasing Ltd, Cambridge helped us to calculate the *BUSTER-TNT* maps. Thomas Schneider is thanked for generously sending us the *ESCET* program. James Bowie and Christopher Thanos supplied us with the coordinates of the monomeric EphB2 SAM domain crystal structure for comparison.

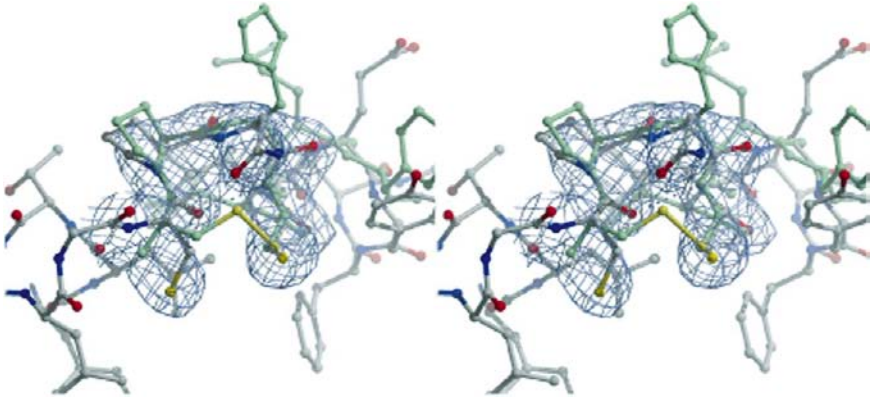

Figure 5
The potential C*XX*C motif in the p73α-SAM crystal structure. The $2mF_o - DF_c$ electron-density map covering Cys502-Pro503-Asn504-Cys505 contoured at 1.0σ is shown. The C*XX*C motif of the oxidized disulfide-bond-formation protein DsbA (PDB code 1fvk; Guddat *et al.*, 1997), coloured light green with the disulfide bond in yellow, is shown superimposed on the p73α structure for comparison.

References

Abrahams, J. P. & Leslie, A. G. W. (1996). *Acta Cryst.* D**52**, 30–42.
Arrowsmith, C. H. (1999). *Cell Death Differ.* **6**, 1169–1173.
Brunger, A. T., Adams, P. D., Clore, G. M., DeLano, W. L., Gros, P., Grosse-Kunstleve, R. W., Jiang, J.-S., Kuszewski, J., Nilges, M., Pannu, N. S., Read, R. J., Rice, L. M., Simonson, T. & Warren, G. L. (1998). *Acta Cryst.* D**54**, 905–921.
Buster Development Group (2001). *BUSTER: A Program for Recovering Missing Phase Information by Bayesian Inference*, http://Lagrange.mrc-lmb.cam.ac.uk/.
Chen, Y. W., Dodson, E. J. & Kleywegt, G. J. (2000). *Structure*, **8**, R213–R220.
Chi, S. W., Ayed, A. & Arrowsmith, C. H. (1999). *EMBO J.* **18**, 4438–4445.

Collaborative Computational Project, Number 4 (1994). *Acta Cryst.* D**50**, 760–763.
Cowtan, K. (1994). *Jnt CCP4 ESF–EACBM Newslett. Protein Crystallogr.* **31**, 34–38.
Davison, T. S., Vagner, C., Kaghad, M., Ayed, A., Caput, D. & Arrowsmith, C. H. (1999). *J. Biol. Chem.* **274**, 18709–18714.
De Laurenzi, V., Costanzo, A., Barcaroli, D., Terrinoni, A., Falco, M., Annicchiarico-Petruzzelli, M., Levrero, M. & Melino, G. (1998). *J. Exp. Med.* **188**, 1763–1768.
Esnouf, R. M. (1997). *J. Mol. Graph.* **15**, 132–134.
Guddat, L. W., Bardwell, J. C. A. & Martin, J. L. (1998). *Structure*, **6**, 757–767.
Guddat, L. W., Bardwell, J. C. A., Zander, T. & Martin, J. L. (1997). *Protein Sci.* **6**, 1148–1156.
Henrick, K. & Thornton, J. M. (1998). *Trends Biochem. Sci.* **23**, 358–361.
Holm, L. & Sander, C. (1996). *Science*, **273**, 595–603.
Jones, T. A., Zou, J. Y., Cowan, S. W. & Kjeldgaard, M. (1991). *Acta Cryst.* A**47**, 110–119.
Jost, C. A., Marin, M. C. & Kaelin, W. G. Jr (1997). *Nature (London)*, **389**, 191–194.
Kaelin, W. G. Jr (1999). *Oncogene*, **18**, 7701–7705.
Kaghad, M., Bonnet, H., Yang, A., Creancier, L., Biscan, J.-C., Valent, A., Minty, A., Chalon, P., Lelias, J.-M., Dumont, X., Ferrara, P., McKeon, F. & Caput, D. (1997). *Cell*, **90**, 809–819.
Laskowski, R. A., MacArthur, M. W., Moss, D. S. & Thornton, J. M. (1993). *J. Appl. Cryst.* **26**, 283–291.
Laue, T. M., Shah, B. D., Ridgeway, T. M. & Pelletier, S. L. (1992). *Analytical Ultracentrifugation in Biochemistry and Polymer Science*, edited by S. R. Harding, A. J. Rowe & J. C. Horton, pp. 90–125. Cambridge: The Royal Society of Chemistry.
Levrero, M., De Laurenzi, V., Costanzo, A., Sabatini, S., Gong, J., Wang, J. Y. J. & Melino, G. (2000). *J. Cell. Sci.* **113**, 1661–1670.
Lohrum, M. A. E. & Vousden, K. H. (2000). *Trends Cell Biol.* **10**, 197–202.
Marin, M. C. & Kaelin, W. G. Jr (2000). *Biochim. Biophys. Acta*, **1470**, M93–M100.
Martin, J. L. (1995). *Structure*, **3**, 245–250.
Merritt, E. A. & Bacon, D. J. (1997). *Methods Enzymol.* **277**, 505–524.
Ozaki, T., Naka, M., Takada, N., Tada, M., Sakiyama, S. & Nakagawara, A. (1999). *Cancer Res.* **59**, 5902–5907.
Poget, S. F., Legge, G. B., Proctor, M. R., Butler, P. J., Bycroft, M. & Williams, R. L. (1999). *J. Mol. Biol.* **290**, 867–879.
Ponstingl, H., Henrick, K. & Thornton, J. M. (2000). *Proteins*, **41**, 47–57.
Ponting, C. P. (1995). *Protein Sci.* **4**, 1928–1930.
Read, R. J. (1986). *Acta Cryst.* A**42**, 140–149.
Rice, L. M. & Brünger, A. T. (1994). *Proteins*, **19**, 277–290.
Schneider, T. R. (2000). *Acta Cryst.* D**56**, 714–721.
Schultz, J., Ponting, C. P., Hofmann, K. & Bork, P. (1997). *Protein Sci.* **6**, 249–253.
Slupsky, C. M., Gentile, L. N., Donaldson, L. W., Mackereth, C. D., Seidel, J. J., Graves, B. J. & McIntosh, L. P. (1998). *Proc. Natl Acad. Sci. USA*, **95**, 12129–12134.
Smalla, M., Schmieder, P., Kelly, M., Ter Laak, A., Krause, G., Ball, L., Wahl, M., Bork, P. & Oschkinat, H. (1999). *Protein Sci.* **8**, 1954–1961.
Stapleton, D., Balan, I., Pawson, T. & Sicheri, F. (1999). *Nature Struct. Biol.* **6**, 44–49.
Stein, E., Cerretti, D. P. & Daniel, T. O. (1996). *J. Biol. Chem.* **271**, 23588–23593.
Thanos, C. D. & Bowie, J. U. (1999). *Protein Sci.* **8**, 1708–1710.
Thanos, C. D., Faham, S., Goodwill, K. E., Cascio, D., Phillips, M. & Bowie, J. U. (1999). *J. Biol. Chem.* **274**, 37301–37306.
Thanos, C. D., Goodwill, K. E. & Bowie, J. U. (1999). *Science*, **283**, 833–836.
Ueda, Y., Hijikata, M., Takagi, S., Chiba, T. & Shimotohno, K. (1999). *Oncogene*, **18**, 4993–4998.
Wang, W. K., Proctor, M. R., Buckle, A. M., Bycroft, M. & Chen, Y. W. (2000). *Acta Cryst.* D**56**, 769–771.
Wright, P. E. & Dyson, H. J. (1999). *J. Mol. Biol.* **293**, 321–331.
Yang, A., Kaghad, M., Wang, Y., Gillett, E., Fleming, M. D., Dötsch, V., Andrews, N. C., Caput, D. & McKeon, F. (1998). *Mol. Cell*, **2**, 305–316.
Zaika, A. I., Kovalev, S., Marchenko, N. D. & Moll, U. M. (1999). *Cancer Res.* **59**, 3257–3263.